Journal of Computational Physics 229 (2010) 8211–8223

Contents lists available at ScienceDirect

Journal of Computational Physics

journal homepage: www.elsevier.com/locate/jcp

A high accuracy algorithm for 3D periodic electromagnetic scattering

Mike Nicholas *

Mathematics Department, Tulane University, 6823 St. Charles Ave, New Orleans, LA 70118, USA

ARTICLE INFO

Article history:
Received 28 May 2009
Received in revised form 2 June 2010
Accepted 21 July 2010
Available online 1 August 2010

Keywords:
Periodic scattering
Periodic Helmholtz Green's function
Ewald method
Müller integral equation

ABSTRACT

We develop a highly accurate numerical method for scattering of 3D electromagnetic waves by doubly periodic structures. We approximate scattered fields using the Müller boundary integral formulation of Maxwell's equations. The accuracy is achieved as singularities are isolated through the use of partitions of unity, leaving smooth, periodic integrands that can be evaluated with high accuracy using trapezoid sums. The removed singularities are resolved through a transformation to polar coordinates. The method relies on the ideas used in the free space scattering algorithm of Bruno and Kunyansky.

1. Introduction

Recent advances have led to electromagnetic scattering algorithms that are both very fast and very accurate. Unfortunately, these do not translate directly to periodic scattering problems due to the difficulties of working with the periodic Helmholtz Green's function. Here we present a highly accurate algorithm for doubly periodic scattering problems. The algorithm is based on the accurate free space scattering algorithm of Bruno and Kunyansky [3–5].

Boundary integral methods in periodic scattering problems must deal with two numerical issues: (1) The periodic Green's function is an infinite series that converges too slowly to be of practical use, and (2) singularities in the integrals limit the accuracy in standard numerical schemes. We use the Ewald summation method [8] to deal with the first of these issues (see [14] for a survey of other techniques). The free space scattering method of [4] overcomes the second obstacle through the use of a partition of unity to separate singularities and a change of variables to smooth singularities. Our algorithm follows the same basic outline. The periodic Green's function, however, does not lend itself as easily to this treatment as the free space Green's function does. Since we use Ewald splitting to accelerate convergence of the periodic Green's function, we must identify and analyze the singularities in the Ewald sums.

In [4], the algorithm is developed for single- and double-layer potentials. We work here with the full Müller integral equations. These include the layer potentials of [4], but they also include other integrals involving second derivatives of the Green's functions. We show that the method applies to all the integrals in the full boundary integral representation of Maxwell's equations.

Periodic scattering problems are of interest to electrical engineers and physicists who apply them to photonic crystal lattices [6,18,9,13,22]. The propagation of waves through such lattices is sensitive to the crystals' geometry, their material properties, and the nature of the incident waves. The recent numerical and experimental discoveries of resonances in transmission have generated interest in periodic electromagnetic scattering problems [7,25,10].

* Tel.: +1 504 862 3438.
E-mail address: mnichol@tulane.edu

0021-9991/$ - see front matter © 2010 Elsevier Inc. All rights reserved.
doi:10.1016/j.jcp.2010.07.028

Much numerical work investigating these problems and resonances has been done in the 2D case [23,12,21,20], but less has been done in 3D. We have previously presented a third order accurate algorithm based on the smoothing of singular integrands and the addition of correction terms to the resulting integrals [16]. The algorithm presented here is more accurate and requires fewer Green's function computations.

1.1. Formulation of the problem

We seek solutions to the Helmholtz equation:

$$\Delta \mathbf{E} + k^2(\mathbf{x})\mathbf{E} = 0 \quad \Delta \mathbf{H} + k^2(\mathbf{x})\mathbf{H} = 0 \tag{1}$$

for

$$k^2(\mathbf{x}) = \begin{cases} k_1^2 = \omega^2 \epsilon_1 \mu_1 & \text{for } \mathbf{x} \notin \Omega \\ k_2^2 = \omega^2 \epsilon_2 \mu_2 & \text{for } \mathbf{x} \in \Omega \end{cases}$$

with divergence conditions

$$\nabla \cdot \mathbf{E} = 0 \quad \nabla \cdot \mathbf{H} = 0 \tag{2}$$

The scatterer Ω is a smooth doubly periodic domain in $\mathbb{R}^3$ whose electromagnetic properties ϵ_2 and μ_2 differ from those of the outside medium ϵ_1 and μ_1. We will take $\epsilon_1 = \mu_1 = \mu_2 = 1$ for the bulk of this paper. The method here presented, however, is valid for general constants in $\mathbb{C}$.

We use scatterers Ω that are 2π periodic in the x and y directions and of finite thickness in the z direction. Generalization to any period is not difficult. The method is valid for general smooth surfaces. The periodic Green's function allows us to do all of our calculations on just one period in both x and y of the scatterer. From this point on, we will let Ω and $\partial\Omega$ refer to just one periodic block of the scatterer.

We distinguish various fields with subscripts. The fields $\mathbf{E}_{inc.}$ and $\mathbf{H}_{inc.}$ are the incident fields that would exist in the absence of the scatterer. Subscripts *int* and *ext* refer respectively to the fields in and out of Ω. Fields $\mathbf{E}_{scatt}$ and $\mathbf{H}_{scatt}$ are scattered fields and are defined outside of Ω as $\mathbf{E}_{scatt} = \mathbf{E}_{ext} - \mathbf{E}_{inc.}$ and $\mathbf{H}_{scatt} = \mathbf{H}_{ext} - \mathbf{H}_{inc.}$.

We require that boundary conditions of tangential continuity be satisfied on $\partial\Omega$:

$$\mathbf{n} \times \mathbf{E}_{ext} = \mathbf{n} \times \mathbf{E}_{int} \quad \mathbf{n} \times \mathbf{H}_{ext} = \mathbf{n} \times \mathbf{H}_{int} \tag{3}$$

where $\mathbf{n}$ is the outward unit normal to Ω. The scattered fields must also satisfy radiation conditions, which ensure that the fields propagate and decay properly while maintaining periodicity. We require the scattered fields to have the form

$$\begin{aligned} \mathbf{E}_{scatt} &= \sum_{m,n} \mathbf{E}^{\pm}_{mn} e^{-\sqrt{-\lambda_{mn}}|z|} e^{i(m+\alpha)x + i(n+\beta)y} \\ \mathbf{H}_{scatt} &= \sum_{m,n} \mathbf{H}^{\pm}_{mn} e^{-\sqrt{-\lambda_{mn}}|z|} e^{i(m+\alpha)x + i(n+\beta)y} \end{aligned} \tag{4}$$

Throughout this paper, all sums of this form are from $-\infty$ to ∞. Here $\lambda_{mn} = k^2 - (m+\alpha)^2 - (n+\beta)^2$, and $\mathbf{E}^{\pm}_{mn}$ and $\mathbf{H}^{\pm}_{mn}$ are constant vectors. The constants α and β depend on the fields' angles of incidence and are defined in Section 1.1.2. The negative sign in the exponentials ensures that the modes decay whenever $\mathrm{Re}(\sqrt{-\lambda_{mn}})$ is nonzero. If, however, $\mathrm{Re}(\sqrt{-\lambda_{mn}}) = 0$, we must choose $\mathrm{Im}(\sqrt{-\lambda_{mn}}) < 0$ so that the waves propagate in the correct direction (from negative to positive z). We adopt the same sign conventions for the modes of the Green's function that will be introduced in Section 1.3.

There exist frequencies for which λ_{mn} can equal zero. These frequencies correspond transmission resonances known as Wood's anomalies [24,25,10]. Green's functions for the problem at such values are undefined, and we therefore avoid these frequencies in our computations. Certain types of resonances known as Wood's anomalies can occur at frequencies close to these singular frequencies [24,25,10].

1.1.1. The incident wave

We will always take the incident wave to be a plane wave propagating from the negative z to positive z direction. The direction of the incident wave is given by the unit vector $\vec{\gamma} = (\gamma_1, \gamma_2, \gamma_3)$. With azimuthal angle θ and polar angle from the z-axis ϕ, $\vec{\gamma}$ is

$$\begin{pmatrix} \gamma_1 \\ \gamma_2 \\ \gamma_3 \end{pmatrix} = \begin{pmatrix} \cos\theta \sin\phi \\ \sin\theta \sin\phi \\ \cos\phi \end{pmatrix}$$

with $0 \leqslant \phi < \frac{\pi}{2}$. For a plane wave, the electric and magnetic fields are contained in planes perpendicular to the direction of propagation $\vec{\gamma}$. The directions of polarization

$$\vec{u_\theta} = \frac{\frac{d\vec{\gamma}}{d\theta}}{\left|\frac{d\vec{\gamma}}{d\theta}\right|} = \begin{pmatrix} -\sin\theta \\ \cos\theta \\ 0 \end{pmatrix} \quad \text{and} \quad \vec{u_\phi} = \frac{\frac{d\vec{\gamma}}{d\phi}}{\left|\frac{d\vec{\gamma}}{d\phi}\right|} = \begin{pmatrix} \cos\theta\cos\phi \\ \sin\theta\cos\phi \\ -\sin\phi \end{pmatrix}$$

define these planes. The electric and magnetic fields must be linear combinations of these two vectors. An incident electric field and corresponding magnetic field satisfy

$$\mathbf{E}_{inc}(x,y,z) = e^{ik_1\vec{\gamma}\cdot\mathbf{x}}[a\vec{u_\theta} + b\vec{u_\phi}] \quad \mathbf{H}_{inc}(x,y,z) = e^{ik_1\vec{\gamma}\cdot\mathbf{x}}[b\vec{u_\theta} - a\vec{u_\phi}]$$

for constants a and b.

Often, we are interested in normally incident plane waves. A normally incident ($\vec{\gamma} = (0,0,1)$) ϕ-polarized electric field with a θ-polarized magnetic field has the form

$$\mathbf{E}_{inc} = e^{ik_1\vec{\gamma}\cdot\mathbf{x}}\vec{u_\phi} = \begin{pmatrix} e^{ik_1 z} \\ 0 \\ 0 \end{pmatrix} \quad \mathbf{H}_{inc} = e^{ik_1\vec{\gamma}\cdot\mathbf{x}}\vec{u_\theta} = \begin{pmatrix} 0 \\ e^{ik_1 z} \\ 0 \end{pmatrix} \tag{5}$$

1.1.2. Pseudoperiodicity of the fields

Our incident fields are not quite periodic. Since $\epsilon_1 = \mu_1 = 1$, the products $k_1\gamma_1$ and $k_1\gamma_2$ are real valued and can be written as

$$k_1\gamma_1 = \hat{m} + \alpha \quad \text{and } k_1\gamma_2 = \hat{n} + \beta$$

for some integers $\hat{m}$ and $\hat{n}$ and some constants $\alpha, \beta \in (-\frac{1}{2}, \frac{1}{2}]$. The constants α and β depend on k_{ext} and on the angles of incidence ϕ and θ. Since $\vec{\gamma}$ is a unit vector, we can write γ_3 in terms of α and β

$$\gamma_3 = \frac{\sqrt{k_1^2 - (\hat{m}+\alpha)^2 - (\hat{n}+\beta)^2}}{k_1}$$

Our electric field becomes

$$\mathbf{E}_{inc}(x,y,z) = e^{i(\alpha x+\beta y)}e^{i\hat{m}x + i\hat{n}y + i\sqrt{k_1^2-(\hat{m}+\alpha)^2-(\hat{n}+\beta)^2}z}[a\vec{u_\theta} + b\vec{u_\phi}]$$

The phasor function

$$e^{i(\alpha x+\beta y)}$$

is not necessarily 2π periodic in x and y. The incident fields are products of a phasor function and a doubly periodic function, and we call them pseudoperiodic.

For normally incident fields, the constants α and β are both zero, and the fields are periodic and not merely pseudoperiodic.

1.2. The Müller integral equations

We will use the boundary integral equations derived by Müller in [15] for free space scattering problems. The adaption of these equations to periodic problems is outlined in [16]. We define the surface currents of the electric and magnetic fields on $\partial\Omega$ to be

$$\mathbf{j}' = \mathbf{n}\times\mathbf{E} \quad \mathbf{j} = -\mathbf{n}\times\mathbf{H}$$

The equations are a set of coupled equations for $\mathbf{j}$ and $\mathbf{j}'$:

$$\begin{aligned}
\mathbf{j}_{inc}(\mathbf{x}') &= \frac{\mu_1+\mu_2}{2\mu_1}\mathbf{j}(\mathbf{x}') \\
&\quad - \frac{1}{\mu_1}\int_{\partial\Omega}\mathbf{n}(\mathbf{x}')\times\left[\mathbf{j}(\mathbf{x})\times\nabla\left(\mu_1 G^{ext} - \mu_2 G^{int}\right)\right]dS(\mathbf{x}) \\
&\quad - \frac{i}{\mu_1\omega}\int_{\partial\Omega}[\mathbf{n}(\mathbf{x}')\times\mathbf{j}'(\mathbf{x})]\left(k_1^2 G^{ext} - k_2^2 G^{int}\right)dS(\mathbf{x}) \\
&\quad - \frac{i}{\mu_1\omega}\int_{\partial\Omega}\mathbf{n}(\mathbf{x}')\times\left[(\mathbf{j}'(\mathbf{x})\cdot\nabla)\nabla(G^{ext} - G^{int})\right]dS(\mathbf{x}) \\
\mathbf{j}'_{inc}(\mathbf{x}') &= \frac{\epsilon_1+\epsilon_2}{2\epsilon_1}\mathbf{j}'(\mathbf{x}') \\
&\quad - \frac{1}{\epsilon_1}\int_{\partial\Omega}\mathbf{n}(\mathbf{x}')\times\left[\mathbf{j}'(\mathbf{x})\times\nabla\left(\epsilon_1 G^{ext} - \epsilon_2 G^{int}\right)\right]dS(\mathbf{x}) \\
&\quad - \frac{i}{\epsilon_1\omega}\int_{\partial\Omega}[\mathbf{n}(\mathbf{x}')\times\mathbf{j}(\mathbf{x})]\left(k_1^2 G^{ext} - k_2^2 G^{int}\right)dS(\mathbf{x}) \\
&\quad - \frac{i}{\epsilon_1\omega}\int_{\partial\Omega}\mathbf{n}(\mathbf{x}')\times[(\mathbf{j}(\mathbf{x})\cdot\nabla)\nabla(G^{ext} - G^{int})]dS(\mathbf{x})
\end{aligned} \tag{6}$$

Here G^{ext} and G^{int} refer to the Green's functions using k_1 and k_2, respectively (see Section 1.3). The Green's functions that appear in the equations without an argument are evaluated at $\mathbf{x}' - \mathbf{x}$. We will call the first and fourth integrals on the right hand side double layer potentials. This is not strictly consistent with the literature, but they do behave as double layer potentials in terms of singularities. The second and fifth integrals are single layer potentials, and we will call the third and sixth integrals the second derivative integrals. Note that these second derivative integrals are singular but not hypersingular since there is a reduction of singularity due to the subtraction $G^{ext} - G^{int}$.

These integral equations are Fredholm of the second kind and are therefore well-posed for the interior currents given the incident fields. Once we have the interior surface currents, we can use interior and exterior representation theorems to find the scattered and the interior electric and magnetic fields:

$$\begin{aligned}
\mathbf{E}_{int}(\mathbf{x}') &= \int_{\partial\Omega} [i\omega\mu_2 \mathbf{j}(\mathbf{x}) G^{int} - \mathbf{j}'(\mathbf{x}) \times \nabla G^{int} + \frac{1}{\epsilon_2} (\mathbf{j}(\mathbf{x}) \cdot \nabla) \nabla G^{int}] dS(\mathbf{x}) \\
\mathbf{H}_{int}(\mathbf{x}') &= \int_{\partial\Omega} [i\omega\epsilon_2 \mathbf{j}'(\mathbf{x}) G^{int} + \mathbf{j}(\mathbf{x}) \times \nabla G^{int} + \frac{1}{\mu_2} (\mathbf{j}'(\mathbf{x}) \cdot \nabla) \nabla G^{int}] dS(\mathbf{x}) \\
\mathbf{E}_{scatt}(\mathbf{x}') &= -\int_{\partial\Omega} [i\omega\mu_1 \mathbf{j}(\mathbf{x}) G^{ext} - \mathbf{j}'(\mathbf{x}) \times \nabla G^{ext} + \frac{1}{\epsilon_1} (\mathbf{j}(\mathbf{x}) \cdot \nabla) \nabla G^{ext}] dS(\mathbf{x}) \\
\mathbf{H}_{scatt}(\mathbf{x}') &= -\int_{\partial\Omega} [i\omega\epsilon_1 \mathbf{j}'(\mathbf{x}) G^{ext} + \mathbf{j}(\mathbf{x}) \times \nabla G^{ext} + \frac{1}{\mu_1} (\mathbf{j}'(\mathbf{x}) \cdot \nabla) \nabla G^{ext}] dS(\mathbf{x})
\end{aligned} \tag{7}$$

1.3. Ewald splitting

The periodic Helmholtz Green's function can be represented as either a sum over periodic reflections or a sum over Fourier modes. Both representations are double infinite sums that converge too slowly to be useful computationally. As in [23,12,16], we use Ewald splitting to accelerate the computation of the Green's functions. This method is something of a hybrid, representing the Green's function as a sum of both quickly converging periodic reflections and quickly converging Fourier modes. We have $G = G1 + G2$, where

$$\begin{aligned}
G1(\mathbf{x}' - \mathbf{x}) &= \frac{1}{8\pi^{3/2}} \sum_{\mu,\nu} e^{-2\pi i(\alpha\mu + \beta\nu)} \sum_{\ell=0}^{\infty} \frac{k^{2\ell} \beta^{2\ell-1}}{\ell!} E_{\ell+\frac{1}{2}} \left(\frac{R_{\mu\nu}^2}{4\beta^2} \right) \\
G2(\mathbf{x}' - \mathbf{x}) &= \frac{1}{8\pi^{5/2}} \sum_{m,n} P_{mn} \sum_{\ell=0}^{\infty} \frac{(-1)^{\ell} (z' - z)^{2\ell}}{4^{\ell} \ell! \beta^{2\ell-1}} E_{\ell+\frac{1}{2}}(-\lambda_{mn}\beta^2)
\end{aligned} \tag{8}$$

where E_n denotes the n^{th} order exponential integral function (see Section 2 and [1]) and where

$$\begin{aligned}
R_{\mu,\nu}^2 &= (x' - x + 2\pi\mu)^2 + (y' - y + 2\pi\nu)^2 + (z' - z)^2 \\
P_{mn} &= e^{im(x'-x) + in(y'-y)} \\
\lambda_{mn} &= k^2 - m^2 - n^2
\end{aligned}$$

In the $G2$ sums, the exponential integral functions must be chosen with the same sign conventions as in the radiation conditions (4). The $G1$ sums contain all of the singularity of the Green's function, and the $G2$ sums are smooth.

The splitting parameter β must be small to ensure rapid convergence in the $G1$ sums and large to ensure rapid convergence in the $G2$ sums. We use FFTs to accelerate the computation of the $G2$ sums over m, n, and thus we can use a relatively small β. After some experimentation, we have seen that $\beta = 0.5$ works well for the range of frequencies presented in the results of Section 6. See [23,17], and [16] for more details on Ewald splitting as applied to this scattering problem.

2. Exponential integrals

The sums $G1$ and $G2$ in the Ewald form of the Green's function (8) include exponential integral functions. The functions that appear in our Green's functions are all of half integer orders of at least $-\frac{1}{2}$. The following facts from [1] allow us to compute all needed exponential integral functions in terms of error functions (we use the fast algorithm of [19] for the complex error functions):

$$\begin{aligned}
E_{\frac{1}{2}}(x) &= \sqrt{\frac{\pi}{x}} \operatorname{erfc}(\sqrt{x}) \\
E_{n+1}(x) &= \frac{1}{n} [e^{-x} - x E_n(x)] \\
E_{-\frac{1}{2}}(x) &= \frac{1}{2x} \left[E_{\frac{1}{2}}(x) + 2e^{-x} \right] \\
\frac{d}{dx} [E_n(x)] &= -E_{n-1}(x)
\end{aligned} \tag{9}$$

The recursive formula for higher order integral equations is sufficient for most applications, but in our case we need an explicit representation for orders greater than $\frac{1}{2}$. We have developed the following representation which can be proved by induction:

$$E_{\ell+\frac{1}{2}}(x) = \frac{(-2x)^\ell}{(2\ell-1)!!}\sqrt{\frac{\pi}{x}}\operatorname{erfc}(\sqrt{x}) + e^{-x}\sum_{k=1}^{\ell} 2^k(-x)^{k-1}\frac{(2(\ell-k)-1)!!}{(2\ell-1)!!} \tag{10}$$

3. The Green's function

Our method requires that we identify and separate the singular and smooth (meaning C^∞) parts of $G1$ (8). All singularities and discontinuities occur when the argument of the exponential integrals is zero. In the $\ell = 0$ term, we have

$$E_{\frac{1}{2}}\left(\frac{r^2}{4\beta^2}\right) = \frac{2\beta\sqrt{\pi}}{r}\operatorname{erfc}\left(\frac{r}{2\beta}\right) = \frac{2\beta\sqrt{\pi}}{r}\left(1-\operatorname{erf}\left(\frac{r}{2\beta}\right)\right)$$

This term appears to be singular, but the function $\operatorname{erf}(r)/r$ is analytic. We therefore have smooth and singular parts of this term:

$$E^{smooth}_{\frac{1}{2}}\left(\frac{r^2}{4\beta^2}\right) = -\frac{2\beta\sqrt{\pi}}{r}\operatorname{erf}\left(\frac{r}{2\beta}\right)$$
$$E^{sing}_{\frac{1}{2}}\left(\frac{r^2}{4\beta^2}\right) = \frac{2\beta\sqrt{\pi}}{r}$$

Required derivatives of the Green's function involve exponential integrals of order $-\frac{1}{2}$. From (9), we have

$$E_{-\frac{1}{2}}\left(\frac{r^2}{4\beta^2}\right) = \frac{2\beta^2}{r^2}\left[2e^{-\frac{r^2}{4\beta^2}} + \frac{2\beta\sqrt{\pi}}{r}\left(1-\operatorname{erf}\left(\frac{r}{2\beta}\right)\right)\right]$$

We similarly have both smooth and singular parts of this function:

$$E^{smooth}_{-\frac{1}{2}}\left(\frac{r^2}{4\beta^2}\right) = \frac{4\beta^2 r e^{-\frac{r^2}{4\beta^2}} - 4\beta^3\sqrt{\pi}\operatorname{erf}\left(\frac{r}{2\beta}\right)}{r^3}$$
$$E^{sing}_{-\frac{1}{2}}\left(\frac{r^2}{4\beta^2}\right) = \frac{4\beta^3\sqrt{\pi}}{r^3} \tag{11}$$

The $\ell > \frac{1}{2}$ exponential integrals are continuous, but they are not smooth (their derivatives are discontinuous). From (10), we have

$$E_{\ell+\frac{1}{2}}\left(\frac{r^2}{4\beta^2}\right) = \frac{(-2)^\ell\sqrt{\pi}}{(2\ell-1)!!}r^{2\ell-1}\left(1-\operatorname{erf}\left(\frac{r}{2\beta}\right)\right) + e^{-\frac{r^2}{4\beta^2}}\sum_{k=1}^{\ell}2^k\left(-\frac{r^2}{4\beta^2}\right)^{k-1}\frac{(2(\ell-k)-1)!!}{(2\ell-1)!!} \tag{12}$$

The odd terms in r are not smooth. Once again, we separate into smooth and singular parts:

$$E^{smooth}_{\ell+\frac{1}{2}}\left(\frac{r^2}{4\beta^2}\right) = -\frac{(-2)^\ell\sqrt{\pi}}{(2\ell-1)!!}r^{2\ell-1}\operatorname{erf}\left(\frac{r}{2\beta}\right) + e^{-\frac{r^2}{4\beta^2}}\sum_{k=1}^{\ell}2^k\left(-\frac{r^2}{4\beta^2}\right)^{k-1}\frac{(2(\ell-k)-1)!!}{(2\ell-1)!!}$$

$$E^{sing}_{\ell+\frac{1}{2}}\left(\frac{r^2}{4\beta^2}\right) = \frac{(-2)^\ell\sqrt{\pi}}{(2\ell-1)!!}r^{2\ell-1}$$

We write the Green's function as $G = G_{smooth} + G_{sing}$, where

$$G_{smooth}(\mathbf{x}'-\mathbf{x}) = \frac{1}{8\pi^{3/2}}\sum_{|\mu|+|\nu|\neq 0}\sum_{\ell=0}^{\infty}\frac{k^{2\ell}\beta^{2\ell-1}}{\ell!}E_{\ell+\frac{1}{2}}\left(\frac{R^2_{\mu\nu}}{4\beta^2}\right) + \frac{1}{8\pi^{3/2}}\sum_{\ell=0}^{\infty}\frac{k^{2\ell}\beta^{2\ell-1}}{\ell!}E^{smooth}_{\ell+\frac{1}{2}}\left(\frac{r^2}{4\beta^2}\right) + G2(\mathbf{x}'-\mathbf{x})$$

$$G_{sing}(\mathbf{x}'-\mathbf{x}) = \frac{1}{8\pi^{3/2}}\sum_{\ell=0}^{\infty}\frac{k^{2\ell}\beta^{2\ell-1}}{\ell!}E^{sing}_{\ell+\frac{1}{2}}\left(\frac{r^2}{4\beta^2}\right)$$

Various derivatives and combinations of Green's functions are needed in the integral Eq. (6). We separate and define all needed forms of the Green's functions similarly.

4. The numerical method

As in [4], we use the smooth partition of unity

$$P(\mathbf{x}'-\mathbf{x}) = \begin{cases} 1, & r \leqslant cA \\ \exp\left(\frac{2e^{-1/u}}{u-1}\right), & cA < r \leqslant A \\ 0, & A \leqslant r \end{cases} \tag{13}$$

where $r = \sqrt{(x'-x)^2 + (y'-y)^2}$ and $u = \frac{r-cA}{A-cA}$ to isolate the singularity in the integral equations. We must have $A < \pi$ and $c < 1$ (we use $A = 2\pi/3$ and $c = 0.3$ for the results of Section 6). We will illustrate the method on a scalar single layer potential

$$\int_{\partial\Omega} G(\mathbf{x}'-\mathbf{x})\phi(\mathbf{x})ds = \int_{\partial\Omega} (1-P)G(\mathbf{x}'-\mathbf{x})\phi(\mathbf{x})ds + \int_{\partial\Omega} PG_{smooth}(\mathbf{x}'-\mathbf{x})\phi(\mathbf{x})ds + \int_{\partial\Omega} PG_{sing}(\mathbf{x}'-\mathbf{x})\phi(\mathbf{x})ds$$

The first of the integrands on the right is smooth, since the partition of unity removes the singularity. This integrand is also periodic. We can therefore evaluate this integral with a trapezoid sum and expect very high accuracy. The second of these integrands is also periodic, since the partition of unity forces it to zero within the periodic block $\partial\Omega$. Since this integrand is also smooth, we can again achieve high accuracy with the trapezoid rule. The final integrand is singular and requires additional analysis.

4.1. The singular integrals

We convert the singular integrals to polar coordinates as in [4]. Let $x' - x = -\rho\cos\theta$ and $y' - y = -\rho\sin\theta$. We can rewrite the singular integral in polar coordinates:

$$\int_{\partial\Omega} PG_{sing}(\mathbf{x}'-\mathbf{x})\phi(\mathbf{x})ds = \frac{1}{2}\int_0^{2\pi}\int_{-A}^{A} P(\rho,\theta)G_{sing}(\rho,\theta)\phi(\rho,\theta)|\rho|d\rho d\theta$$

For a fixed θ, the $d\rho$ integral is periodic due to the partition of unity. Our G_{sing} function contains $1/r$ singularities and non-smooth $r^{2\ell-1}$ terms. The product $\frac{|\rho|}{r}$, however, is smooth in ρ for a fixed θ. The limit of this function as $\rho \to 0$ is

$$L = \lim_{\rho\to 0}\frac{|\rho|}{r} = \sqrt{\frac{1}{1+(f_x\cos\theta + f_y\sin\theta)^2}} \tag{14}$$

The $|\rho|r^{2\ell-1}$ terms are also smooth. The $d\rho$ integrals can therefore be computed with high order convergence using a trapezoid rule. The $d\theta$ integrals are clearly periodic and smooth. We can therefore approximate the single layer potential with high order convergence. By symmetry, we can perform the θ integration from *0* to π.

4.2. Polar interpolation

We use the iterative method GMRES to approximate solutions to the integral equations. In this process, we have approximations to $\mathbf{j}$ and $\mathbf{j}'$ on the rectangular grid $x_i = 2\pi i/N$, $y_j = 2\pi j/N$, $i, j = 0, 1, \ldots, N-1$. The method for dealing with the singular integrals, however, requires having approximations to these functions on points of a polar coordinate grid. To overcome this obstacle, we use the same fast, accurate interpolation scheme introduced in [4]. For a fixed θ, our method requires that we integrate along the line $x = x' + \rho\cos\theta$, $y = y' + \rho\sin\theta$. We discretize ρ along this line, and we choose $\Delta\rho$ so that each ρ_j lies on a line of the rectangular grid. For $\theta \in [\pi/4, 3\pi/4]$, we choose $\Delta\rho = \Delta y/\sin\theta$, and the ρ_j lie on lines y_j. As we perform GMRES iterations on the integral equation, we have values for the integrand at x_i values along these y_j lines, so we can perform one dimensional interpolation along each of these lines to approximate the required values of the integrand. We perform this high accuracy interpolation along a line y_j in three steps:

- Use a fast Fourier transform (FFT) on the x_i values of the integrand to obtain the Fourier coefficients of the integrand. Since the function is periodic, this has a very high accuracy.
- Use these Fourier coefficients to evaluate the integrand on a much finer grid (as in [4] we use a grid that is 16 times finer that the original grid). The FFT is again used to quickly and accurately obtain these values.
- We need a value of the integrand that lies between points on the refined grid. To obtain this, we construct a third degree interpolating polynomial between the fine grid points. We choose the polynomial so that it matches the trigonometric polynomial in value and in first derivative at the endpoints of the interval. This approach was used in [4] with excellent results. A super-algebraic interpolation scheme could be developed at this point, but with the highly accurate interpolated values from the FFTs and with the small grid size of the refined grid, the fourth order accuracy of this polynomial interpolation is sufficient for practical purposes (for a grid with $N = 32$ points, errors will be on the order of 10^{-8}).

We thus have a fast and accurate way to obtain the values needed for the polar integration. If $\theta \notin [\pi/4, 3\pi/4]$, we set $\Delta\rho = \Delta x/\cos\theta$, and the ρ_i lie on lines x_i. The interpolation is performed similarly, but we interpolate y values along these lines of constant x. Refer to [4] for more details.

4.3. Adapting the method to the Müller integral equations

To this point, we have only outlined the method for a scalar single layer potential. The idea of method is the same for each of the integrals of the Müller equation (6), but there are various derivatives and singularities involved. We will show how the method works for each of the four types of integral in (6).

4.3.1. The single layer potential

We have already outlined the method for a scalar single layer potential. There are two vector valued single layer potentials in the integral equations of the form

$$\int_{\partial\Omega} [\mathbf{n}(\mathbf{x}') \times \mathbf{j}(\mathbf{x})] \left(k_1^2 G^{ext} - k_2^2 G^{int} \right) dS(\mathbf{x})$$

To evaluate these integrals with a trapezoid sum, we need limits in both the smooth and singular parts at $r = 0$. For the smooth integral, we need

$$\lim_{r\to 0} E_{\frac{1}{2}}^{smooth}\left(\frac{r^2}{4\beta^2}\right) = -2 \tag{15}$$

The singular part of this integral is computed in polar coordinates, and we need

$$\lim_{\rho\to 0} |\rho| E_{\frac{1}{2}}^{sing}\left(\frac{r^2}{4\beta^2}\right) = 2\beta\sqrt{\pi}L \tag{16}$$

in the $d\rho$ integral, where L is the limit (14). As seen, the other nonsmooth parts of the integrand smoothly go to zero after the change to polar coordinates.

4.3.2. The double layer potential

The integral

$$\int_{\partial\Omega} \mathbf{n}(\mathbf{x}') \times [\mathbf{j}(\mathbf{x}) \times \nabla \left(\epsilon_1 G^{ext} - \epsilon_2 G^{int} \right)] dS(\mathbf{x})$$

is singular and behaves somewhat like a double layer potential. The smooth part of the integral is zero at the origin and is computed in rectangular coordinates with a trapezoid sum. The most singular part of this integrand comes from the exponential integral of order $-\frac{1}{2}$. From (11), we see that we must look at the triple product

$$\mathbf{n}(\mathbf{x}') \times [\mathbf{j}(\mathbf{x}) \times (\mathbf{x}' - \mathbf{x})] \frac{4\beta^3\sqrt{\pi}}{r^3}$$

The normal vector $\mathbf{n}$ and tangential vector $\mathbf{j}$ are

$$\mathbf{n}(\mathbf{x}') = \frac{1}{\sqrt{1 + f_x^2 + f_y^2}} \begin{pmatrix} f_x \\ f_y \\ -1 \end{pmatrix}$$

$$\mathbf{j}(\mathbf{x}) = \begin{pmatrix} j_1(x,y) \\ j_2(x,y) \\ j_1(x,y) f_x(x,y) + j_2(x,y) f_y(x,y) \end{pmatrix}$$

where the functions without arguments are evaluated at (x', y'). For small r, we expand the functions in $\mathbf{j}$ in a Taylor series centered at (x', y'). The triple product becomes

$$\frac{4\beta^3\sqrt{\pi}}{r^3\sqrt{1 + f_x^2 + f_y^2}} (\mathbf{v}(\mathbf{x}' - \mathbf{x}, \mathbf{y}' - \mathbf{y}) + O(r^3))$$

where

$$v_1 = \left(\frac{f_{xx}}{2}(x' - x)^2 - \frac{f_{yy}}{2}(y' - y)^2 \right) j_1 + (f_{xy}(x' - x)^2 + f_{yy}(x' - x)(y' - y)) j_2$$

$$v_2 = (f_{xx}(x'-x)(y'-y) - f_{xy}(y'-y)^2)j_1 + \left(\frac{f_{yy}}{2}(y'-y)^2 - \frac{f_{xx}}{2}(x'-x)^2\right)j_2$$

$$v_3 = \left(\frac{f_{xx}f_x}{2}(x'-x)^2 - \frac{f_{yy}f_x}{2}(y'-y)^2 + f_{xx}f_y(x'-x)(y'-y) + f_{xy}f_y(y'-y)^2\right)j_1$$
$$+ \left(\frac{f_{yy}f_y}{2}(y'-y)^2 - \frac{f_{xx}f_y}{2}(x'-x)^2 + f_{yy}f_x(x'-x)(y'-y) + f_{xy}f_x(x'-x)^2\right)j_2$$

As in the case of the single layer potential, we change to polar coordinates. We have the limit

$$\lim_{\rho\to 0}\frac{4\beta^3\sqrt{\pi}}{\sqrt{1+f_x^2+f_y^2}}\frac{\rho^2|\rho|}{r^3}(\mathbf{v}(\theta)+O(r)) = \frac{4\beta^3L^3\sqrt{\pi}}{\sqrt{1+f_x^2+f_y^2}}\mathbf{v}(\theta)$$

where L is the limit (14) and

$$v_1 = \left(\frac{f_{xx}}{2}\cos^2\theta - \frac{f_{yy}}{2}\sin^2\theta\right)j_1 + (f_{xy}\cos^2\theta + f_{yy}\cos\theta\ sin\theta)j_2$$

$$v_2 = (f_{xx}\cos\theta\sin\theta - f_{xy}\sin^2\theta)j_1 + \left(\frac{f_{yy}}{2}\sin^2\theta - \frac{f_{xx}}{2}\cos^2\theta\right)j_2$$

$$v_3 = \left(\frac{f_{xx}f_x}{2}\cos^2\theta - \frac{f_{yy}f_x}{2}\sin^2\theta + f_{xx}f_y\cos\theta\sin\theta + f_{xy}f_y\sin^2\theta\right)j_1$$
$$+ \left(\frac{f_{yy}f_y}{2}\sin^2\theta - \frac{f_{xx}f_y}{2}\cos^2\theta + f_{yy}f_x\cos\theta\sin\theta + f_{xy}f_x\cos^2\theta\right)j_2$$

All other nonsmooth parts of this integrand smoothly go to zero at the origin. The integrand is therefore smooth for a fixed θ, and we can thus compute the double layer potential with very high accuracy using the trapezoid rule.

4.3.3. The second derivative integral

We have two integrals of the form

$$\int_{\partial\Omega}\mathbf{n}(\mathbf{x}')\times[(\mathbf{j}(\mathbf{x})\cdot\nabla)\nabla(G^{ext}-G^{int})]dS(\mathbf{x})$$

As mentioned, some of the singularity of these integrals is removed in the difference $(G^{ext}-G^{int})$. For the smooth integrals in rectangular coordinates, the mixed partial derivatives are all 0 at the origin. The other derivatives in the smooth integrals and all of the derivatives in the singular integrals have a nonzero contribution at 0 coming from an exponential integral of order $\frac{1}{2}$. These limits are the same as (15) and (16).

The singular parts of these integrals once again arise from exponential integrals of order $-\frac{1}{2}$, and we again deal with them via the change to polar coordinates. For example, for the mixed partial derivative $(G^{ext}-G^{int})_{xz}$, the most singular piece of the integrand has of the form

$$(x'-x)(z'-z)\frac{4\beta^3\sqrt{\pi}}{r^3} = (x'-x)(f(x',y')-f(x,y))\frac{4\beta^3\sqrt{\pi}}{r^3}$$

For small r, this is

$$(x'-x)(f_x(x'-x)-f_y(y'-y)+O(r^2))\frac{4\beta^3\sqrt{\pi}}{r^3}$$

In polar coordinates, this is once again smooth as $\rho\to 0$ for a fixed θ:

$$4\beta^3\sqrt{\pi}L^3(f_x\cos^2\theta + f_y\cos\theta\sin\theta)$$

The second derivatives are handled similarly, and all other nonsmooth parts of the integrand become smooth with the change to polar coordinates and are zero at the origin. The trapezoid rule therefore yield high accuracy approximations for the second derivative integrals as well.

4.3.4. The nonsingular integral

Since $\mu_1 = \mu_2$, the following integral is not singular

$$\int_{\partial\Omega}\mathbf{n}(\mathbf{x}')\times\left[\mathbf{j}(\mathbf{x})\times\nabla\left(\mu_1G^{ext}-\mu_2G^{int}\right)\right]dS(\mathbf{x})$$

This integrand is 0 at the origin in both the rectangular and polar integrals. There are, of course, still nonsmooth parts of the Green's functions here, and we must still convert to polar coordinates as in the other integrals for these parts.

5. Implementation

5.1. Computing the Green's function

The Ewald summation method described in Section 1.3 greatly accelerates computation of the Green's function. The function is, however, still represented as various infinite sums (8), and computing it is still the most time consuming piece of the algorithm. To accelerate these computations, we first precompute and store factorials and other relevant coefficients in (8). We then group the $G2$ sums as

$$G2(\mathbf{x}' - \mathbf{x}) = \frac{1}{8\pi^{5/2}} \sum_{\ell=0}^{\infty} \frac{(-1)^{\ell}(z'-z)^{2\ell}}{4^{\ell}\ell!\beta^{2\ell-1}} \sum_{m,n} P_{mn} E_{\ell+\frac{1}{2}}(-\lambda_{mn}\beta^2)$$

We compute the inner m, n sums with FTTs and tabulate the results. We use the same number N of frequencies that we use to discretize the surface. Since $G2$ is smooth and periodic, this is more than sufficient to guarantee high accuracy in these sums. This technique, which was recently used in [16] and [2], significantly accelerates the computation of $G2$. With this acceleration in $G2$, we can choose the splitting parameter β small to that only a few of the μ, ν terms are needed in the $G1$ sums. The ℓ sums that remain in $G1$ and $G2$ are both Taylor series for exponentials, and estimates could be derived for the convergence of these sums. We have, however, opted to simply include terms until they fall below a given tolerance (10^{-10}). The results do not differ appreciably when we set the tolerance higher.

5.2. Solving the integral equation

We have outlined a high order integrator for the Müller equations. To actually solve the equations, we iterate using standard GMRES without restarts. Since the integral equation is Fredholm of the second kind, we expect the iterations to be stable. The iterations indeed converge for our test case and other scatterers, and they converge in relatively few iterations (typically, fewer than 50). The system scales as N^2 for N total discretization points. Thus for an $N \times N$ grid, the vector that we iterate has $12N^2$ complex valued entries; the problem becomes computationally large very quickly. It is necessary to tabulate values of the Green's function for use during the iterations.

6. Numerical results

6.1. Integrals with exact surface currents for flat slab test case

The scattering problem with a flat slab scatterer can be solved analytically (see [16]). With this scatterer, the incident and interior currents are known constants on each surface. We evaluate the integrals in (6) using the exact interior surface currents. Results are shown in Table 1.

These results show high accuracy (an improvement of at least two orders of magnitude when doubling N) and convergence. As expected, accuracy decreases as frequency increases. Table 2 shows similar results for a higher frequency.

We use GMRES to approximate solutions to the integral equation. We have an L_∞ norm error of $1.82e-06$ (with $N = 32, \epsilon_2 = 5$, and $\omega = 0.3$).

Table 1
Table of results for evaluation of Müller integrals with a flat slab scatterer using exact internal surface currents ($\omega = 0.3, \epsilon_1 = 5.0, \mathbf{x}' = \mathbf{0}$).

N	$\lvert\mathbf{j}^{exact}(\mathbf{x}') - \mathbf{j}^{numerical}(\mathbf{x}')\rvert$	$\lvert\mathbf{j}'^{exact}(\mathbf{x}') - \mathbf{j}'^{numerical}(\mathbf{x}')\rvert$
32	1.0057e − 06	3.1269e − 06
64	2.5372e − 08	7.8884e − 08
128	2.1007e − 10	6.5302e − 10
256	6.3357e − 14	8.1795e − 14

Table 2
Table of results for evaluation of Müller integrals with a flat slab scatterer using exact internal surface currents with a higher frequency ($\omega = 1.3, \epsilon_1 = 5.0, \mathbf{x}' = \mathbf{0}$).

N	$\lvert\mathbf{j}^{exact}(\mathbf{x}') - \mathbf{j}^{numerical}(\mathbf{x}')\rvert$	$\lvert\mathbf{j}'^{exact}(\mathbf{x}') - \mathbf{j}'^{numerical}(\mathbf{x}')\rvert$
32	5.4467e − 05	6.5079e − 05
64	5.7615e − 07	6.8839e − 07
128	3.9663e − 09	4.7389e − 09
256	2.3773e − 13	7.3508e − 13

6.2. Integrals on curved surface

We apply the algorithm to the surface

$$F_1(x,y) = \frac{1}{5}\sin^2(x/2)\sin^2(y/2) \quad F_2(x,y) = \pi - \frac{1}{5}\sin^2(x/2)\sin^2(y/2)$$

which we call the dimpled surface (the surface of Fig. 1 is a steeper version of this). In Table 3, we see the high order convergence of the integrals for this curved surface. Since we do not know the exact surface currents for this surface, we use the surface currents for the flat slab surface as if they were the first iteration in our GMRES solver. We use the approximation with $N = 256$ as our "exact" reference for these results.

If we compare differences with $N = 32$, $N = 64$, $N = 128$, we have the ratios

$$\frac{|\mathbf{j}_{N=32} - \mathbf{j}_{N=64}|}{|\mathbf{j}_{N=64} - \mathbf{j}_{N=128}|} = 108.07 \quad \frac{|\mathbf{j}'_{N=32} - \mathbf{j}'_{N=64}|}{|\mathbf{j}'_{N=64} - \mathbf{j}'_{N=128}|} = 110.17$$

These ratios, for the incident surface currents with $\omega = 0.3$ and $\epsilon_2 = 15$ evaluated at $\mathbf{x}' = 0$, indicate high order convergence.

6.3. The full integral equation

Having seen good convergence in the individual integrals, we look at approximating solutions to the integral Eq. (6).

6.3.1. Transmission coefficient

A quantity of interest in scattering problems is the transmission coefficient T. This is a comparison of the energy in the incident fields to that in the total external fields far from the scatterer. The Poynting vector

$$\mathbf{S} = \overline{\mathbf{E}} \times \mathbf{H},$$

with $\overline{\mathbf{E}}$ the complex conjugate of $\mathbf{E}$, is a measurement of an electromagnetic field's energy flux [11]. For any surface F far from the scatterer Ω and normal to the incident fields, we define the incident and transmitted energy flows by

$$U_{inc} = \int_F Re(\mathbf{S}_{inc}(\mathbf{x}) \cdot \mathbf{n}(\mathbf{x}))dS(\mathbf{x}) \quad U_{tran} = \int_F \mathrm{Re}(\mathbf{S}_{ext}(\mathbf{x}) \cdot \mathbf{n}(\mathbf{x}))dS(\mathbf{x})$$

where $\mathbf{n}$ is an outward unit normal to F. These flows are measures of the energy passing through the surface F. The transmission coefficient is defined as

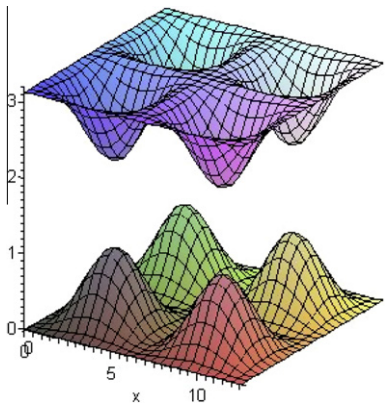

Fig. 1. A few periods of a sample surface. This surface is 2π periodic in x and y and has finite thickness in z.

Table 3
Table of results for evaluation of Müller integrals with a dimpled scatterer using the $N = 256$ results as an "exact" baseline ($\omega = 0.3, \epsilon_1 = 5.0, \mathbf{x}' = \mathbf{0}$).

N	$\lvert\mathbf{j}^{exact}(\mathbf{x}') - \mathbf{j}^{numerical}(\mathbf{x}')\rvert$	$\lvert\mathbf{j}'^{exact}(\mathbf{x}') - \mathbf{j}'^{numerical}(\mathbf{x}')\rvert$
32	9.7164e − 07	3.3074e − 06
64	2.5965e − 08	7.5899e − 08
128	2.1456e − 10	6.2927e − 10

$$T = \sqrt{\frac{U_{tran}}{U_{inc}}} \tag{17}$$

In computing T, we take the surface F to be far enough from Ω that the decaying modes of the field are negligible, so that only the propagating modes contribute to the integrals. The transmission coefficient is relevant physically, but it is also an important quantity numerically, since it requires the full solution of the integral equations.

6.3.2. Flat slab scatterer

The transmission coefficient for the flat slab scatterer can be computed analytically. The results for this test case (In Table 4) show high accuracy in solving the integral equation.

6.3.3. Corrugated roof scatterer

We solve the integral equation for the surface

$$F_1(x,y) = \frac{1}{5}\sin^2(x/2) \quad F_2(x,y) = \pi - \frac{1}{5}\sin^2(x/2)$$

which we call the corrugated roof surface. Upon calculating the surface currents, we use (7) to get the scattered fields. From the fields, we can compute the transmission coefficient. The results (in Table 5) show fast convergence of transmission coefficients

6.3.4. Wood's anomaly resonance

Current interest in periodic scattering is partially due to the desire to study transmission resonance phenomena. It has been observed [16] that Wood's anomaly resonances can occur for frequencies close to the singular frequencies that occur in the Green's function. It is important that numerical methods be able to resolve such resonances. Fig. 2 shows transmission coefficient profiles as a function of frequency for the corrugated roof scatterer. There is a resonance in transmission for

Table 4
Table of transmission coefficient results for the flat slab scatterer ($\omega = 0.3, \epsilon_1 = 5.0$). Calculation of the transmission coefficient requires the solution of the full Müller integral equations and the approximation of the scattered electric and magnetic fields at a point.

N	Error in transmission coefficient
32	1.5962e − 6
64	4.0264e − 8

Table 5
Table of transmission coefficient results for the corrugated roof scatterer ($\omega = 0.3, \epsilon_1 = 5.0$).

N	Transmission coefficient
32	0.77265672
64	0.77265853
128	0.77265832

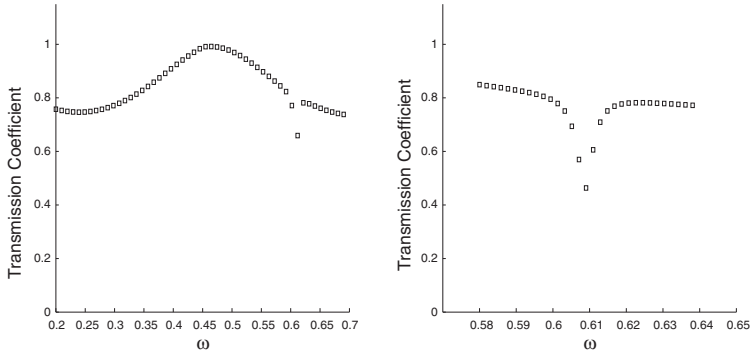

Fig. 2. Transmission coefficient as a function of frequency for the corrugated roof scatterer. On the right is a more finely resolved view of the resonance. ($\epsilon_1 = 5.0$).

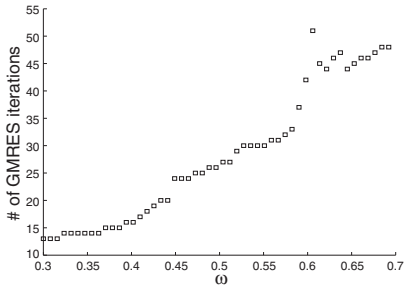

Fig. 3. Number of GMRES iterations as a function of frequency for the corrugated roof scatterer. ($\epsilon_1 = 5.0$).

frequencies just less than the singular value 0.63. On the right is a close up of the resonance, and we see that the method is able to resolve such phenomena.

6.3.5. GMRES iterations

As expected, the number of GMRES iterations increases with frequency (see Fig. 3). Notice that the number jumps at frequencies where the number of penetrating modes increases (at $\omega = 0.45$ and $\omega = 0.63$). We also see that more iterations are required for frequencies near the Wood's anomaly resonance.

7. Conclusions

We have developed a very accurate algorithm for 3D periodic scattering. The method shows high accuracy for both a flat slab test case and for a curved surface. It is a straightforward method that is practical for small problems. For larger problems, calculation of the Green's functions becomes very time consuming. Fast summation methods have made it possible to study even large scale free space scattering problems. The adaption of such methods to the periodic problem is in progress and should be a great improvement.

Acknowledgement

This work was supported in part by NSF VIGRE grant DMS 0239996.

References

[1] Milton Abramowitz, Irene A. Stegun, Handbook of Mathematical Functions with Formulas, Graphs, and Mathematical Tables, ninth dover printing, tenth GPO printing ed., Dover, New York, 1964.
[2] J. Thomas Beale, John Strain, Locally corrected semi-lagrangian methods for stokes flow with moving elastic interfaces, J. Comput. Phys. 227 (8) (2008) 3896–3920.
[3] Oscar P. Bruno, New high-order integral methods in computational electromagnetism, CMES Comput. Model. Eng. Sci. 5 (4) (2004) 319–330.
[4] Oscar P. Bruno, Leonid A. Kunyansky, A fast, high-order algorithm for the solution of surface scattering problems: basic implementation, tests, and applications, J. Comput. Phys. 169 (1) (2001) 80–110.
[5] Oscar P. Bruno, Leonid A. Kunyansky, Surface scattering in three dimensions: an accelerated high-order solver, R. Soc. Lond. Proc. Ser. A Math. Phys. Eng. Sci. 457 (2016) (2001) 2921–2934.
[6] Kokou Dossou, Michael A. Byrne, Lindsay C. Botten, Finite element computation of grating scattering matrices and application to photonic crystal band calculations, J. Comput. Phys. 219 (1) (2006).
[7] T.W. Ebbessen, H.J. Lezec, H.F. Ghaemi, T. Thio, P.A. Wolff, Extraordinary optical transmission through sub-wavelength hole arrays, Nature 391 (1998) 667–669.
[8] P.P. Ewald, Die berechnung optischer und electrostatischer gitterpotentiale, Ann. Phys. 64 (1921) 253–287.
[9] S. Fan, J.D. Joannopoulos, Analysis of guided resonance in photonic crystal slabs, Phys. Rev. B 65 (2002).
[10] Lan Gao, Junichi Nakayama, Scattering of a TM plane wave from periodic random surfaces, Waves Random Media 9 (1999) 53–67.
[11] David Griffiths, Introduction to Electrodynamics, Prentice Hall, 1999.
[12] Mansoor A. Haider, Stephen P. Shipman, Stephanos Venakides, Boundary-integral calculations of two-dimensional electromagnetic scattering in infinite photonic crystal slabs: channel defects and resonances, SIAM J. Appl. Math. 62 (6) (2002) 2129–2148 (electronic).
[13] Steven G. Johnson, Shanhui Fan, Pierre R. Villeneuve, J.D. Joannopoulos, Guided modes in photonic crystal slabs, Phys. Rev. B 60 (8) (2002) 5751–5758.
[14] C.M. Linton, The Green's function for the two-dimensional Helmholtz equation in periodic domains, J. Eng. Math. 33 (4) (1998) 377–402.
[15] C. Müller, Foundations of the Mathematical Theory of Electromagnetic Waves, Springer, Berlin, 1969.
[16] Michael J. Nicholas, A higher order numerical method for 3-D doubly periodic electromagnetic scattering problems, Commun. Math. Sci. 6 (3) (2008) 669–694.
[17] Vassilis G. Papanicolaou, Ewald's method revisited: rapidly convergent series representations of certain Green's functions, J. Comput. Anal. Appl. 1 (1) (1999) 105–114.
[18] Giuseppe Pelosi, Alessandro Cocchi, Stafano Selleri, Electromagnetic scattering from infinite periodic structures with a localized impurity, IEEE Trans. Antennas Propag. 49 (5) (2001) 697–702.
[19] G.P.M. Poppe, C.M.J. Wijers, Algorithm 680: evaluation of the complex error function, ACM Trans. Math. Software 16 (1) (1990) 47.
[20] S. Shipman, S. Venakides, Resonant transmission near nonrobust periodic slab modes, Phys. Rev. E 71 (2005). 026611(1–10).
[21] Stephen P. Shipman, Stephanos Venakides, Resonance and bound states in photonic crystal slabs, SIAM J. Appl. Math. 64 (1) (2003) 322–342 (electronic).

[22] V.G. Solov'ev, C.M. Torres, S.G. Romanov, Reflection, transmission, and scattering of light by photonic crystals based on opal films, Russ. Phys. J. 47 (3) (2004) 286–292.
[23] Stephanos Venakides, Mansoor A. Haider, Vassilis Papanicolaou, Boundary integral calculations of two-dimensional electromagnetic scattering by photonic crystal Fabry–Perot structures, SIAM J. Appl. Math. 60 (5) (2000) 1686–1706 (electronic).
[24] R.W. Wood, On the remarkable case of uneven distribution of a light in a diffraction grating spectrum, Philos. Mag. 4 (1902) 396–402.
[25] V.V. Zalipaev, M.M. Popov, Wood's anomalies in a problem of the diffraction of a planar wave by a smooth periodic boundary. Zap. Nauchn. Sem. Leningrad. Otdel. Mat. Inst. Steklov. (LOMI), 186 (1990) (Mat. Vopr. Teor. Rasprostr. Voln. 20, 87–100, 182).